scientific reports

Check for updates

OPEN

Presence and absence of intrinsic magnetism in graphitic carbon nitrides designed through C–N–H building blocks

Teerachote Pakornchote, Annop Ektarawong, Akkarach Sukserm, Udomsilp Pinsook & Thiti Bovornratanaraks✉

We use the first principle calculation to investigate the intrinsic magnetism of graphitic carbon nitrides (GCNs). By preserving three-fold symmetry, the GCN building blocks have been built out of different combinations between 6 components which are C atom, N atom, s-triazine, heptazine, heptazine with C atom at the center, and benzimidazole-like component. That results in 20 phases where 11 phases have been previously reported, and 9 phases are newly derived. The partial density of states and charge density have been analyzed through 20 phases to understand the origin of the presence and absence of intrinsic magnetism in GCNs. The intrinsic magnetism will be present not only because the GCNs comprising of radical components but also the π-conjugated states are not the valence maximum to break the delocalization of unpaired electrons. The building blocks are also employed to study alloys between g-C_3N_4 and g-C_4N_3. The magnetization of the alloys has been found to be linearly dependent on a number of C atoms in the unit cell and some magnetic alloys are energetically favorable. Moreover, the intrinsic magnetism in GCNs can be promoted or demoted by passivating with a H atom depending on the passivated positions.

Various types of 2-dimensional (2D) materials have been explored their magnetism that suite for spintronics and magnetic devices. For metal-free materials, 2D organic frameworks such as triangulenes and graphitic carbon nitrides (GCNs) are candidates that possess intrinsic magnetism with high Curie temperature and high flexibility[1–4]. Organic radicals can be linked by a triazine which is a carbon-nitride ring stabilizing paramagnetic 2D organic frameworks[5]. The triangulene which is a fragment of graphene can be scaled its magnetization by increasing a size of the fragment[6,7]. It can be crystallized by connecting its edges with other chemical groups[8]. For graphene, each C atom spends 3 electrons to form σ bonds and leaves one electron forming conjugated π bond suppressing graphene's magnetism while the magnetism in triangulenes exists due to lack of π conjugation. Accordingly, the magnetism of 2D organic frameworks can be suppressed by a delocalization of electrons in π orbitals affected by compressive strain[9].

The intrinsic magnetism in graphene can be risen by a defect producing a half-filled band of π orbitals[10]. The defects can be either voids or impurities splitting the spin-up and spin-down p_z states at the Fermi level (E_F) and inducing a magnetic moment[11–14]. One method used to create void defects in graphene is by doping N atoms where the voids are surrounded by N atoms, then N-doped graphene becomes magnetic[15,16]. Although, high doping, void, and passivation concentrations lead to phase instability limiting amounts of spin density in graphene[17–19].

In this work, we focus on GCNs whose several magnetic and non-magnetic phases have been predicted. For instance, g-C_4N_3 is a magnetic phase with one Bohr magneton (μ_B) per unit cell[20,21], and $C_{14}N_{12}$ bears $2\mu_B$ per unit cell of magnetization[4]. C_9N_7 and $C_{10}N_9$ are magnetic phases while C_3N_2, C_4N, and C_9N_4 are non-magnetic[4,15]. Their magnetism arises from an unpaired electron contributing a magnetic moment to a system. The structure that has two unpaired electrons can be non-magnetic or magnetic depending on they are in singlet or triplet states, respectively[22,23]. Anyhow, magnetic GCNs have not yet achieved in experiments. The GCN that is typically synthesized are g-C_3N_4, but it is non-magnetic. It is in a form of s-triazine or heptazine networks and a candidate for photocatalysis and carbon dioxide adsorbing materials[24–31]. Some extra-treatments have been

Extreme Conditions Physics Research Laboratory and Center of Excellence in Physics of Energy Materials(CE:PEM), Department of Physics, Faculty of Science, Chulalongkorn University, Bangkok 10330, Thailand. ✉email: thiti.b@chula.ac.th

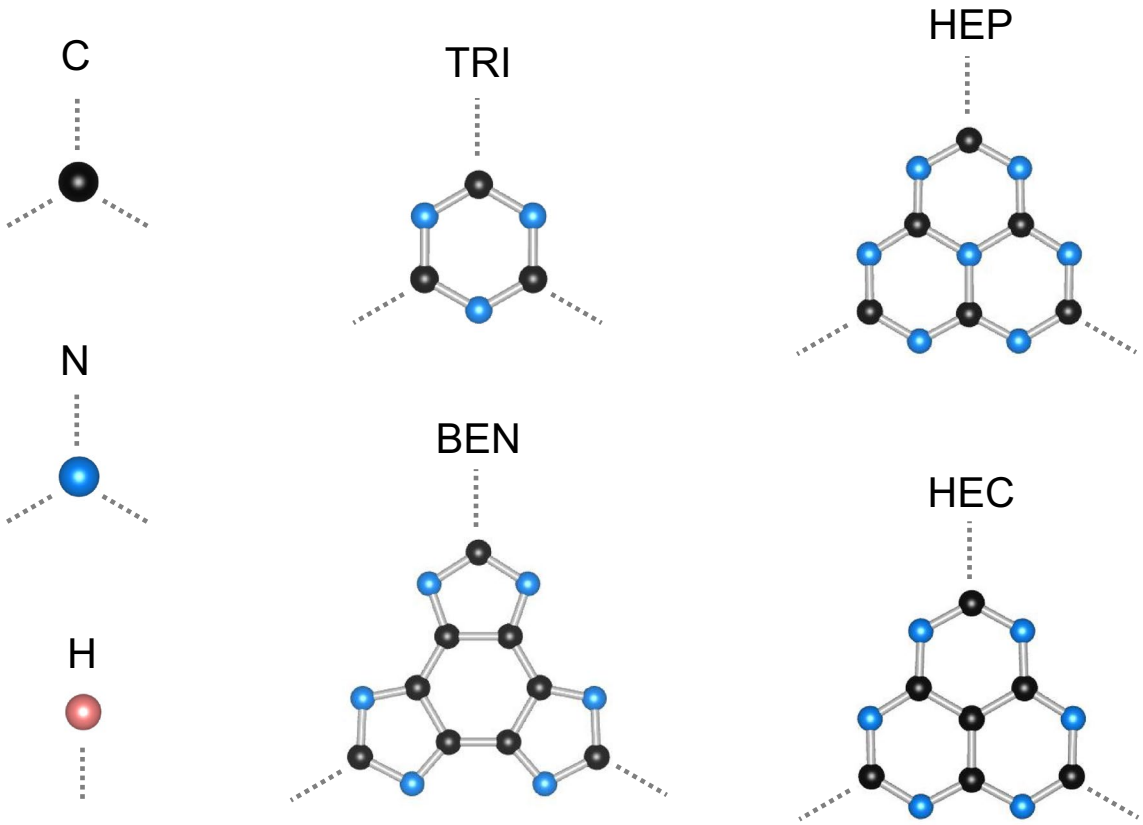

Figure 1. Components of building blocks with three-fold connecting parts except for H atom that has one connecting part shown as grey dotted lines.

used to activate the intrinsic magnetism of this phase[32,33]. For example, the magnetism in GCNs can be enhanced by defects, hydrogenation, and fluorination[34–40]. GCNs are particularly porous, so a metal atom can sit in a hole and induces magnetism of the structure[41,42]. The metal atom can also be a linkage connecting atoms and build blocks, but the Curie temperature is not as high as a light-atomic linkage[43,44].

Herein, we present an aspect that structures of GCNs can be constructed from building blocks of C–N assisting us to understand the presence and absence of intrinsic magnetism of GCNs. The construction is focused on the building block whose two components are connecting together with three-fold symmetry. The first principle method based on spin-polarized density functional theory (DFT) has been employed to study thermodynamics stability, electronic structure and magnetism of GCNs. The absence and presence of intrinsic magnetism of GCNs have been analyzed through their electronic structures. We propose two mechanisms playing a crucial role in GCNs magnetism; firstly, one out of two components in the building block must have a free radical, and secondly, π conjugation does not present near the Fermi energy if both components have free radicals. We also present a series of study on hydrogenated and alloy GCNs; the GCNs prefer to be passivated by a H atom at some locations able to activate or deactivate the intrinsic magnetism, and the magnetization of GCNs can be modified by mixing different building blocks.

Results and discussion

Building blocks. The building blocks are C, N, H, s-triazine (TRI), heptazine (HEP and HEC) and tetracyclic benzimidazole (BEN) components where HEC is a heptazine with C atom at the center instead of N atom (see Fig. 1). Each component will be joint with other components in three directions preserving three-fold symmetry except for H atom that will be only dangling with C and N atoms. One can think of an alloy which is a mixture of several components; however, this work is limited to study connections between two types of components where the first component is a *core*, and the second component is a *connector*. Therefore, in this study, GCNs are constructed from cores which are TRI, HEP, HEC and BEN, and connectors which are C, N, TRI, and HEP while a H atom is neither a core nor a connector but a passivating atom. GCNs are typically labeled by a tuple of numbers of C and N atoms, (n_C, n_N), in a unit cell which is sometimes ambiguous, so they are, instead, designated as *core-connector*, e.g. TRI-N whose common name is g-C_3N_4 is a structure where TRI is a core and N is a connector.

By our constructions, there are 20 phases reported here; 11 phases, to the best of our knowledge, have been reported before[4,20,21,24–29,29,45–52], and 9 phases which are HEP–TRI, HEP–HEP, HEC-C, HEC–HEP, and BEN-X (X = C, TRI, HEP, HEC, and BEN) are newly derived by this study (see Fig. S1 in Supplementary Information). Table 1 presents the formation energy (E_{form}) of all phases which are entirely positive in the order of hundreds

		Cores					
		C	N	TRI	HEP	HEC	BEN
Connectors	C	0	735	417	309	373	399
	N		0	313	265	300	386
	TRI			1368	243	304	378
	HEP				228	273	329
	HEC					313	372
	BEN						376

Table 1. The E_{form} of each GCN is reported in meV per atom unit where each column and row are core and connector components, respectively. The blue–white–red colors are shaded according to the values from lowest to highest. N–N, in contrast, denotes a N_2 molecule.

		Cores					
		C	N	TRI	HEP	HEC	BEN
Connectors	C	0.00	0.00	1.00	1.00	0.01	0.00
	N		–	0.00	0.00	1.00	1.00
	TRI			0.00	0.00	1.00	1.00
	HEP				0.00	1.00	1.00
	HEC					2.00	0.45
	BEN						0.00

Table 2. The magnetization of each GCN is reported in μ_B unit where each column and row are core and connector components, respectively. The parity of the n_e of each phase is labeled by blue and yellow denoting odd and even, respectively.

meV by comparing with the energy of graphene and N_2 molecule. Noting that GCNs can be synthesized from chemical compounds, e.g., melamine, melam, and melon, so their E_{form} would change according to precursors.

Figure S2 in Supplementary Information shows that the E_{form} seems to decrease with respect to N concentration. However, it is not a good presentation because different types of GCNs are being compared. Bu et al.[19] shows that the formation energy of N-doped graphene and GCNs with pyridinic N increase similarly with amount of N concentration up to 0.25%. The former starts increasing higher if N concentration is more than 0.3%. The structures with pyrrolic N also have formation energy higher than the structures with pyridinic N. In this work, TRI, HEP, and HEC are components with pyridinic N, while BEN is a component with pyrrolic N. The formation energy of structures with BEN component is thus higher than that of structures without BEN component. The formation energy of structures with HEP component are lower than that of structures with HEC component even HEP is a N-doped HEC. The structures with N connector are more energetically favorable than those with C connector.

TRI–TRI has the highest E_{form} among other phases. The C–N–C angle of TRI component is ideally 120°. It is 108.4° in TRI–TRI while it is about 114° to 120.5° in other structures whose the TRI component is constituent. This angle in TRI–TRI that is much sharper than other phases may cause high strain on the structure throwing the E_{form} of TRI–TRI to 1.368 eV.

Magnetic and electronic properties. The intrinsic magnetism in GCNs is present or absent due to combinations between cores and connectors. Table 2 presents the magnetizations of GCNs where each phase is constructed from the core and the connector labeled in each column and row, respectively. Since the core and the connector are commutable, the values below diagonal should be the same as the values above diagonal. Most phases, whose intrinsic magnetism are present, have either HEC or BEN as components except for HEC-C, BEN-C and BEN–BEN that are non-magnetic. Two more magnetic phases are TRI-C and HEP-C. The magnetism is absent in C–C, C–N, TRI-N, HEP-N and HEP–HEP where C–C and C–N are graphene and 2D honeycomb carbon nitride, respectively. Noting that N–N is a N_2 molecule, so it is disregarded.

We count a number of valence electrons, which do not form σ bonds, per unit cell (n_e) of each phase in order to understand a key factor governing presence or absence of the intrinsic magnetism. In a honeycomb structure, a C atom covalently bonds with its three nearest atoms leaving one lone electron, while a N atom leaves two electrons which is a lone pair. In TRI, HEP, HEC, and BEN, the pyridinic and pyrrolic N atoms bonding with only two nearest atoms have $n_e = 3$; therefore, TRI and HEP have even n_e considered to be non-magnetic components, and HEC and BEN have odd n_e considered to be magnetic components. We expect that if the n_e is even, all electrons left over from σ bonding will pair together suppressing the intrinsic magnetism of the structure. In contrast, if the n_e is odd, a single electron will be a free radical granting a magnetic moment. The parity of the n_e of each phase is presented in Table 2 and labeled in blue if the n_e is odd and yellow if the n_e is even. As labeled, the GCNs are magnetic or non-magnetic if the n_e are odd or even, respectively, except for C–N, HEC–HEC and BEN–HEC. The magnetic behavior of the excepted phases, in contrast, can be explained through the projected

		Cores					
		C	N	TRI	HEP	HEC	BEN
Connectors	C	SM	M	2.15 (0)	1.92 (0.31)	SM	SM
	N		-	1.56	1.17	2.06 (0.17)	SM
	TRI			0.87	1.53	2.08 (0)	0.12 (0.61)
	HEP				1.21	1.77 (1.54)	0.11 (0.49)
	HEC					2.47 (0)	M
	BEN						SM

Table 3. The energy gap of each GCN is reported in eV unit where each column and row are core and connector components, respectively. The spin-up (x) and spin-down (y) energy gaps are reported in a x (y) form if they are discrepant but are reported in a single value if they are the same. The electronic behaviors are denoted as M for metals and SM for semi-metals.

DOS (PDOS) and the localization of the charge density. The intrinsic magnetism of GCNs is then discussed separately for each core component in subsections below. The PDOS will be shown by types of atoms where C_A and N_A denote C and N atoms of the A component, respectively.

C-. Particularly, C atoms in graphene spend their three valence electrons to form σ bonds and one valence electron to form conjugated π bonds with the entire structure. Lieb[10] has shown that the net spin is not vanished if numbers of atoms in two sublattices of a bipartite lattice such as graphene are not equal. (Ovchinnikov[53] has proposed the same equation of the net spin for hydrocarbons). The theorem was validated by an existence of magnetic moment in defective and hydrogenated graphenes[13,14]. In this case, C–C is a perfect lattice graphene where the C atoms in two sublattices are equal, so it is non-magnetic.

For C–N (equivalent to N–C in Table 2) which also has a honeycomb structure, lone pairs of N atoms and lone electrons of C atoms form π conjugation without defects suppressing the intrinsic magnetism even the n_e per the unit cell is odd. This is according to the PDOS of CN (see Fig. S3 in Supplementary Information) that the p_z orbitals of C and N atoms dominating the states across the E_F. It is because the p_z electrons delocalize and pair together across several cells even the n_e in the unit cell is odd.

TRI- and HEP-. TRI and HEP components have even n_e, so they themselves obtain no magnetic moment, and their combinations, TRI–TRI, HEP–TRI, and HEP–HEP, consequently, yield no magnetism (see Table 2). TRI-N and HEP-N, whose each N connector leaves one lone pair, are also non-magnetic. In contrast to TRI-C and HEP-C, the C connector has one n_e which is the p_z electron granting a magnetic moment to the whole structures. If that is the case, why does the p_z electron of the C connector not delocalize and pair with p_z electrons of TRI? Because the p_z states of the C connector and C_{TRI} atom are in different energy levels and both are in the same energy levels with p_z states of N_{TRI} atom (see Fig. 2). This is also true in HEP-C, TRI-N and HEP-N. For TRI-N and HEP-N, the p_z electrons of the N connector already form a lone pair, so the levels mismatch does not matter.

For the electronic property, TRI–TRI and TRI-N are semiconductors with energy gaps 0.87 and 1.56 eV, respectively, while TRI-C is a half-metal with spin-up energy gap 2.15 eV (see Table 3). For TRI-C, the p_x and p_y states of N_{TRI} atoms dominate the states around the E_F, and the p_z states of N_{TRI} and the C connector are at a bit below the E_F. The p_z states of C_{TRI} and N_{TRI} atoms hybridize with one another at below − 3 eV which is at different energy level with the p_z states of the C connector (see Fig. 2b). Noting that they appear at the same energy level below − 5 eV, but that is deep from the E_F. This result also holds for TRI-N where the p_z states of the N connector hybridize with that of N_{TRI} atoms at − 2 eV but not with that of C_{TRI} atoms (see Fig. 2d). For TRI–TRI, since its core and connector are the same, main features of its PDOS are similar to TRI of TRI-C and TRI-N that the p_x and p_y states dominate at valence states near the E_F while the p_z states appear at below − 4 eV (see Fig. S4 in Supplementary Information). Besides, in TRI-C and TRI-N, the p_z states of N_{TRI} appear two times; one hybridizes with the p_z states of the connector, and another one hybridizes with the p_z states of C_{TRI} atoms.

Mataga[54] has proposed that the electrons of atoms in the ring (TRI) are paired through the π conjugated bonds leaving their non-bonding σ orbitals and non-bonding π orbital of the C connector to be unpaired. This is in accordance to our result that the spin moment comes from the valence states of the p_x and p_y states of atoms in the ring and the p_z states of the C connector. The p_z states form a narrow band as in Mataga's discussion, but the p_x and p_y states form a wide band.

The HEP-X (X = N, TRI, and HEP) structures whose each component obtains even n_e are non-magnetic semiconductors with 1.17, 1.53, and 1.21 eV for energy gaps, respectively (see Table 3). Since HEP-C is magnetic, it has two energy gaps which are 1.92 and 0.31 for spin-up and spin-down, respectively. The PDOS of HEP-C (HEP-N) shown in Fig. 3 demonstrates the hybridization between atoms in the core and connector similar to that

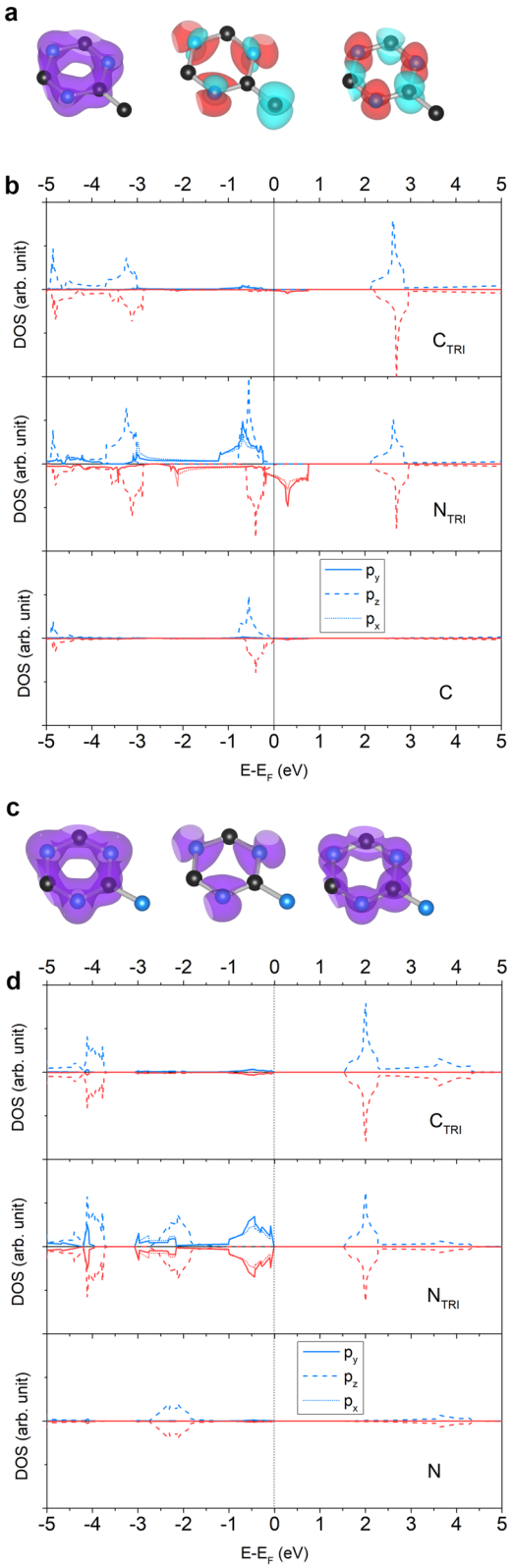

Figure 2. Structures of (**a**) TRI-C and (**c**) TRI-N are illustrated where left, middle, and right figures show isosurfaces of charge density at deep, valence and conduction levels, respectively. The spin-up, spin-down and total chage densities are shown in blue, red, and purple, respectively. The spin-up (blue) and spin-down (red) PDOS of (**b**) TRI-C and (**d**) TRI-N are projected on p_x (dottedline), p_y (solid line) and p_z (solid line) orbitals of C and N atoms.

of TRI-C (TRI-N). For HEP-N, the p_x and p_y DOS between spin-up and spin-down are the same for HEP-N. In contrast, for HEP-C, the feature peak of spin-down DOS shift to above the E_F causing the discrepancy between its spin-up and spin-down DOS. This feature also happens if the PDOS of TRI-C and TRI-N are compared. For HEP–TRI and HEP–HEP (see Figs. S5 and S6 in Supplementary Information), the p_z states of atoms in the core and connector appear at the same energy level below − 2 eV while their p_x and p_y states appear near the E_F.

HEC-. The electronic properties of HEC-X (X = C, N, TRI, HEP, and HEC) shown in Table 3 are various where HEC-C is a semimetal. HEC–TRI and HEC–HEC are a half-metal with 2.08 and 2.47 eV, respectively, for spin-up energy gap. HEC-N (HEC–HEP) is a semiconductor where its spin-up and spin-down energy gaps are 2.06 (1.77) and 0.17 (1.54) eV, respectively. Figure 4d–f show the structures of HEC-C, HEC-N, and HEC–HEC, respectively.

The HEC component has odd n_e; therefore, its combination with the C connector, HEC-C, is non-magnetic while its combinations with N, TRI, and HEP components are magnetic with one μ_B per unit cell. On the one hand, the PDOS of HEC-N (see Fig. 4b) shares similar features to that of TRI-C and HEP-C where the p_x and p_y spin-up (spin-down) states are at valence maximum (conduction minimum) level and the p_z states are at deeper energy level. On the other hand, the PDOS of HEC-C shows a distinguish feature that the p_z states of every atom appear at the valance maximum level while their p_x and p_y states shift to conduction minimum level. Because HEC-C has a number of electrons smaller than HEP-N by two electrons, so the E_F which is a function of number of electrons shifts down from above to below the p_x and p_y PDOS peaks (see Fig. 4a). Moreover, C_{HEC} atoms contribute their p_z states to the valence maximum level in contrast to previous phases, so the p_z orbitals of C_{HEC} and N_{HEC} atoms and the C connector can form conjugated π bonds delocalizing the electrons and suppressing the intrinsic magnetism. For HEC–TRI and HEC–HEP (see Figs. S7 and S8 in Supplementary Information), their PDOS share similar features to HEP–TRI and HEP–HEP, but they are magnetic.

Despite that HEC–HEC has even n_e, it has a magnetization for $2\mu_B$ per unit cell. Here, we run into the second question that why does the reason for the absence of intrinsic magnetism discussed above not be able to use with HEC–HEC? As aforementioned, for TRI, HEP, and HEC components, the p_z states of their C atoms are at deep energy level while the p_z states of their N atoms appear twice, first at shallow level and second at the energy level as C atoms. Even though the π conjugation in HEC–HEC occurs at energy below − 1 eV, only p_z states of N_{HEC} atoms have a contribution near the E_F (see Fig. 4c). The electrons in the valence maximum level hence do not form conjugated π bonds, but localize at the p_x and p_y states of N_{HEC} atoms. HEC–HEC thus obtains $2\mu_B$ per unit cell, one of which comes from each HEC component, and the most discrepancy between spin-up and spin-down DOS is from the p_x and p_y states.

BEN-. The BEN component has odd n_e, so BEN-C and BEN–BEN are non-magnetic, and BEN-X (X = N, TRI, and HEP, HEC) are magnetic with one μ_B per unit cell except for BEN–HEC which has the magnetization about $0.45\mu_B$ per unit cell (see Table 2). For the electronic property, BEN–TRI (BEN–HEP) is a semiconductor with spin-up and spin-down energy gap about 0.12 (0.11) and 0.61 (0.49) eV, respectively, BEN–HEC is a metal, and others are semimetals (see Table 3).

The BEN component contains a C hexagonal ring and three pyrroles (see Fig. 5a–d for structures of BEN-X for X = C, N, HEC, and BEN, respectively). Its PDOS shows that the p_x and p_y states are at energy level lower than the p_z states (see Fig. 5h). Near the E_F, the p_z DOS of C_{BEN} atoms and the p_x and p_y DOS of N_{BEN} atoms are high while DOS of connector $C_{\{TRI,HEP,HEC\}}$ atoms are tiny. Consequently, the valence states of BEN–BEN are dominated by the p_z states of C_{BEN} atoms, and the p_x and p_y states of N_{BEN} atoms appear at lower energy level (see Fig. 5h). For BEN-C, it is non-magnetic, so there is no discrepancy between spin-up and spin-down DOS (see Fig. 5e). Because its number of electrons is smaller than BEN–BEN, so its E_F drops below the p_z states causing the p_x and p_y states are at the valence maximum level. Although, the p_z states of C_{BEN} and N_{BEN} atoms and the C connector appear from the E_F down to − 4 eV showing a sign of the π conjugation but its PDOS near the E_F is tiny (see Fig. 5i).

For BEN-N, the p_z states show the discrepancy between spin-up and spin-down DOS while the p_x and p_y states are slightly discrepant between spin-up and spin-down DOS (see Fig. 5f). Therefore, a spin moment of BEN-N comes from electrons in the p_z states in contrast to, e.g., TRI-C and HEP-C that their spin moments come from electrons in the p_x and p_y states of N atoms. Because BEN-N has a number of electrons higher than BEN-C by one electron, so the E_F shifts to higher than the p_z states becoming the valence maximum. For BEN–TRI and BEN–HEP, their PDOS features near the E_F are from the p_z states which is clearly induced by the BEN component (see Figs. S9 and S10 in Supplementary Information). The p_z states of C_{TRI} atoms show no contribution here while those of C_{HEP} atoms have small contributions. The p_x and p_y states of N_{TRI} and N_{HEP} atoms are discrepant in contrast to the PDOS of phases discussed in previous sections. The spin moments of BEN–TRI and BEN–HEP are also from the electrons in the p_z states which is similar to BEN-N.

For BEN–HEC, its PDOS is a mixing between the characteristics of BEN and HEC components (see Fig. 5g). At the E_F, the spin-up and spin-down DOS are from the p_z states and the p_x and p_y states, respectively, where the former is dominated by the PDOS of C_{BEN} atoms, and the latter is dominated by the PDOS of N_{HEC} and C_{HEC} atoms. The p_z states at the E_F are actually from the PDOS of every atom except C_{HEC} atoms, so the π conjugation does not occur at this level but at below -1.0 eV. Therefore, BEN and HEC components obtain different spin moments where the spin moment of the BEN component is greater.

Summary. The building blocks can be grouped by their PDOS characteristics into three groups which are the atoms, i.e., C and N atoms, the carbon nitride rings, i.e., TRI, HEP, and HEC components, and BEN component. The individual atoms contribute their p_z states as their valence maximum states. The carbon nitride rings have

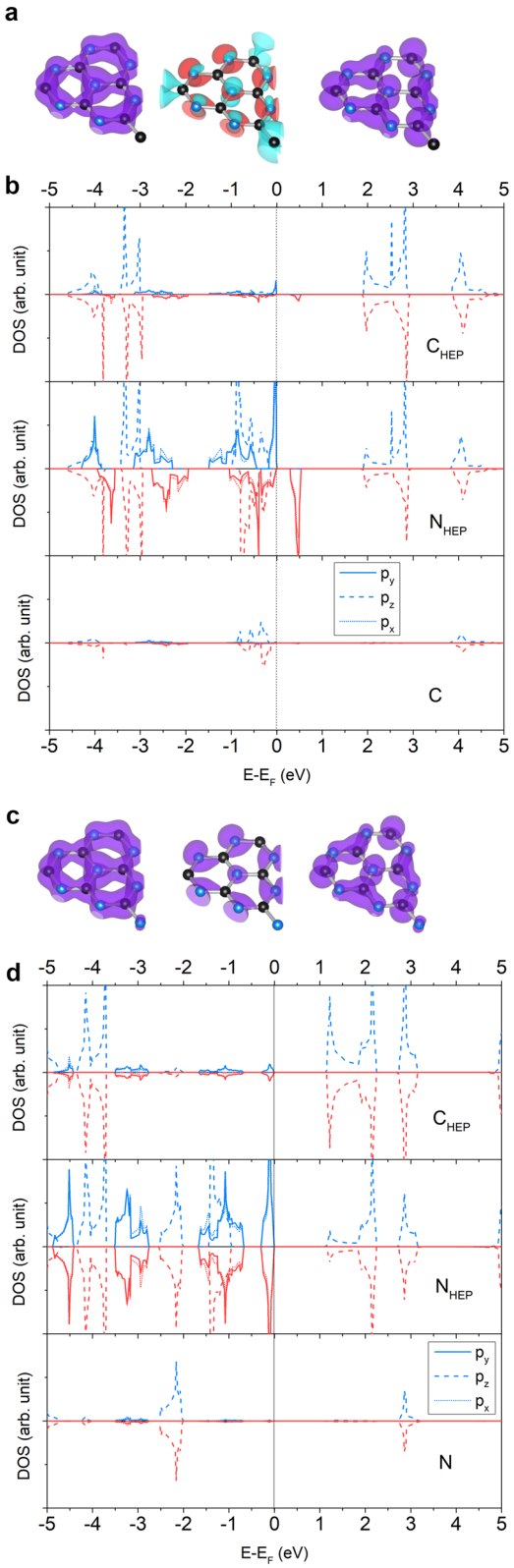

Figure 3. Structures of (**a**) HEP-C and (**c**) HEP-N are illustrated where left, middle, and right figures show isosurfaces of charge density at deep, valence and conduction levels, respectively. The spin-up, spin-down and total chage densities are shown in blue, red, and purple, respectively. The spin-up (blue) and spin-down (red) PDOS of (**b**) HEP-C and (**d**) HEP-N are projected on p_x (dottedline), p_y (solid line) and p_z (solid line) orbitals of C and N atoms.

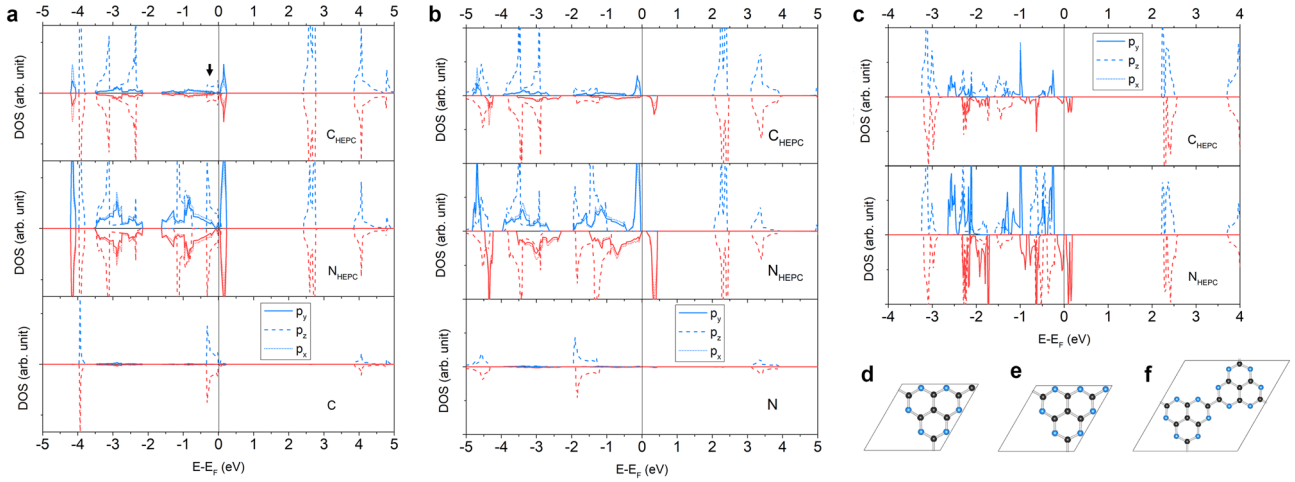

Figure 4. The spin-up (blue) and spin-down (red) PDOS of (**a**) HEC-C, (**b**) HEC-N, and (**c**) HEC–HEC are projected on p_x (dottedline), p_y (solid line) and p_z (solid line) orbitals of C and N atoms. A black arrow points the p_z DOS of C_{HEC}. Structures of (**d**) HEC-C, (**e**) HEC-N, and (**f**) HEC–HEC are illustrated.

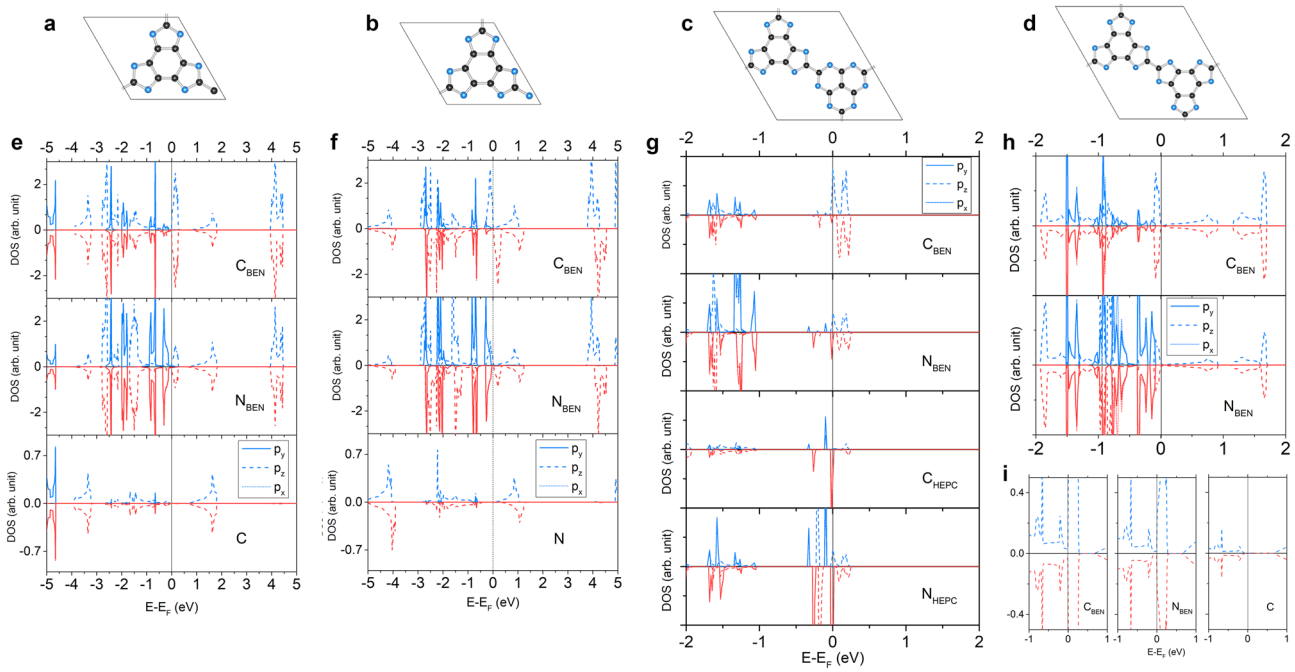

Figure 5. Structures of BEN-X (X = (**a**) C, (**b**) N, (**c**) HEC, and (**d**) BEN) are illustrated. The spin-up (blue) and spin-down (red) PDOS of BEN-X (X = (**e**) C, (**f**) N, (**g**) HEC, and (**h**) BEN) are projected on p_x (dotted line), p_y (solid line) and p_z (solid line) orbitals of C and N atoms. (**i**) The p_z DOS of BEN-C is magnified.

their valence maximum states dominated by the p_x and p_y states of N atoms, and their C and N atoms form π bonds at deeper energy level. The BEN component has the p_z states of C atoms as its valence maximum states and the p_x and p_y states of N atoms at the energy level next to the valence maximum states. If the π conjugation forms across the core and the connector of GCNs near the E_F, the intrinsic magnetism of GCNs will be suppressed. Otherwise, for a structure with odd n_e, the magnetic moment will be localized in the p_x and p_y states (p_z states) of N (C) atoms if the structure is a combination with the carbon nitride rings (BEN component).

Besides, there are three structures which are C–N, HEC–HEC, and BEN–HEC that their magnetism cannot be determined by counting the n_e. The C–N is non-magnetic because of the π conjugation at the valence maximum level. The HPEC–HEC and BEN–HEC, in contrast, lack of the π conjugation at the valence maximum level, so their magnetic moments are localized at each component to the system.

Two factors thereupon playing the important role to raise or demote the intrinsic magnetism of GCNs are the n_e and the π conjugation. The components with odd (even) n_e tend to contribute the unpaired (paired) electrons to the system. Their combinations mostly result in presence and absence of the intrinsic magnetism if the n_e in

the unit cell is odd and even, respectively. For the odd-odd combinations, i.e., C–C, HEC-C, and BEN-C, the p_z orbitals of the core and connector form the conjugated π bonds pairing electrons across the structures. For the odd-even combinations, e.g., TRI-C, HEP-C, and HEC-N, the π conjugation does not occur because the p_z states of the C and N connectors are at the energy level same as (different from) the p_z states of N (C) atoms of the cores. The p_z states of N and C atoms of the cores are also hybridizing at the same energy level but at deeper level. In the even-even case, it does not matter if there are conjugated π bonds near the E_F. The electrons in each component are paired and contribute no magnetic moment.

Alloys. The g-C_3N_4 or TRI-N has been synthesized while the g-C_4N_3 or TRI-C has yet existed only in the simulation[27]. TRI-C is magnetic, but its E_{form} is 133 meV higher than TRI-N (see Table 1). To achieve the intrinsic magnetism, the connectors are alloyed between C and N atoms, so the magnetization can be arisen proportional to a number of C connectors (C_{con}). The structures of the alloy can be represented by different ordered patterns of C and N connectors created up to 42 atoms per primitive cell for 52 structures (including TRI-C and TRI-N) by using Hart and Forcade's algorithm[55] where some of order structures are illustrated in Fig. 6a.

Figure 6b is a plot of ratio between the magnetization and the number of C_{con} in an ordered structure with respect to a ratio between C_{con} and total number of the connectors in the ordered structure. As expected, the magnetization of order structure increases linearly as the number of C_{con} in the structure increasing because each C_{con} contributes a radical to the system. Figure 6c shows that the formation energy of the ordered solid solutions is below zero with respect to those of TRI-N and TRI-C indicating that the connector C and N atoms are likely to be chemically ordered at low temperature in thermodynamic equilibrium. The transition temperature between order-disordered phase that helps to verify a structure found in the experiment, for instance, HEP/TRI-C/N[56], hence needs to be investigated[19], but it is beyond the scope of this work.

Hydrogenation. The intrinsic magnetism of GCNs can be altered by a hydrogenation[39]. Therefore, an atom in each GCN is here passivated by one H atom per unit cell in order to investigate the change in magnetism and the thermodynamically stability. Each GCN has several atomic positions for H atom to passivate, for example, H atom can passivate on C_{TRI}, N_{TRI}, and the C connector of TRI-C which are 3 configurations in total. As a result, the configurations of each GCNs except C–N, that the H atom is passivating with N atoms, have the E_{form} lower than their non-hydrogenated phases. The H atom passivating with C atom of GCNs yields high E_{form} because it induces high strain on the structure while the passivation with N atom is on the side of the structure inducing less strain (see Fig. S11 in Supplementary Information).

Since different configurations yield different results in the magnetizations and the E_{form}, Table 4 shows the magnetization of the configuration of each hydrogenated GCN that has the lowest E_{form}. Noting that the magnetization of hydrogenated graphene (C–C) is one μ_B per unit cell, but it is not reported in Table 4 because its E_{form} is higher than graphene. For hydrogenated HEC-X, the HEC component whose N_{HEC} atom is passivated by H atom has even n_e, so hydrogenated HEC-X obtains one μ_B of magnetization per unit cell for X = C and HEC and zero magnetization for X = N, TRI, and HEP.

For hydrogenated BEN-X, the HEC component whose N_{HEC} atom is passivated by H atom has also even n_e, so hydrogenated BEN-X obtains zero magnetization for X = N, TRI, and HEP. Accordingly, the magnetization of hydrogenated BEN–HEC is one μ_B per unit cell because one of its components has even n_e while another has odd n_e, so the magnetic moments between BEN and HEC are no more annihilated in the hydrogenated case. In contrast, the magnetization of hydrogenated BEN-C is $0.20\mu_B$ per unit cell even its n_e is odd because its valence electrons can be shared through the π conjugation at the valence maximum states.

For hydrogenated TRI-X, the TRI component whose N_{HEC} atom is passivated by H atom has odd n_e, so hydrogenated TRI-X obtains zero magnetization for X = C and 0.84 and 1 μ_B per unit cell for X = N and TRI, respectively. Notwithstanding that hydrogenated HEP-X for X = N, TRI, and HEP obtain odd n_e, their thermodynamically favorable configurations yield zero magnetization.

Conclusions

Firstly, we present building blocks comprising 19 GCNs (and graphene) and the reason behind their emergent intrinsic magnetism through bonding states and charge density. The structure that has even n_e is non-magnetic because all valence electrons are paired suppressing the magnetic moment. The structure that has odd n_e can be either magnetic or non-magnetic depending on the valence maximum states are localized or delocalized, respectively. The valence maximum states are ensured to be localized if they are from the p_x and p_y orbitals but are not necessary to be delocalized if they are from the p_z orbitals. The p_z orbitals of every atom in the core and connector must present in the valence maximum states to form the π conjugation; otherwise, the unpaired electron will be localized in its component (core or connector) producing the magnetic moment.

Secondly, we also apply the building-blocks scheme to study alloys mixing between g-C_3N_4 and g-C_4N_3. The magnetization of the alloy increases linearly as a concentration of the C connector, and some promising alloys are energetically favorable. Lastly, a H atom attached on GCN lowers the E_{form} of the structure. The H atom can change the magnetization of the system depending on a position it is passivating. Therefore, these understandings could lead to the future design for stable GCNs that maintain to be radicals with magnetism.

Methods

The VASP package[57,58] used to perform a first principle calculation based on spin-polarized density functional theory (DFT) has been employed to study the structural, electronic, and magnetic properties of GCNs. In the spin-polarized DFT, the charge density and the magnetization density can be written as[59]

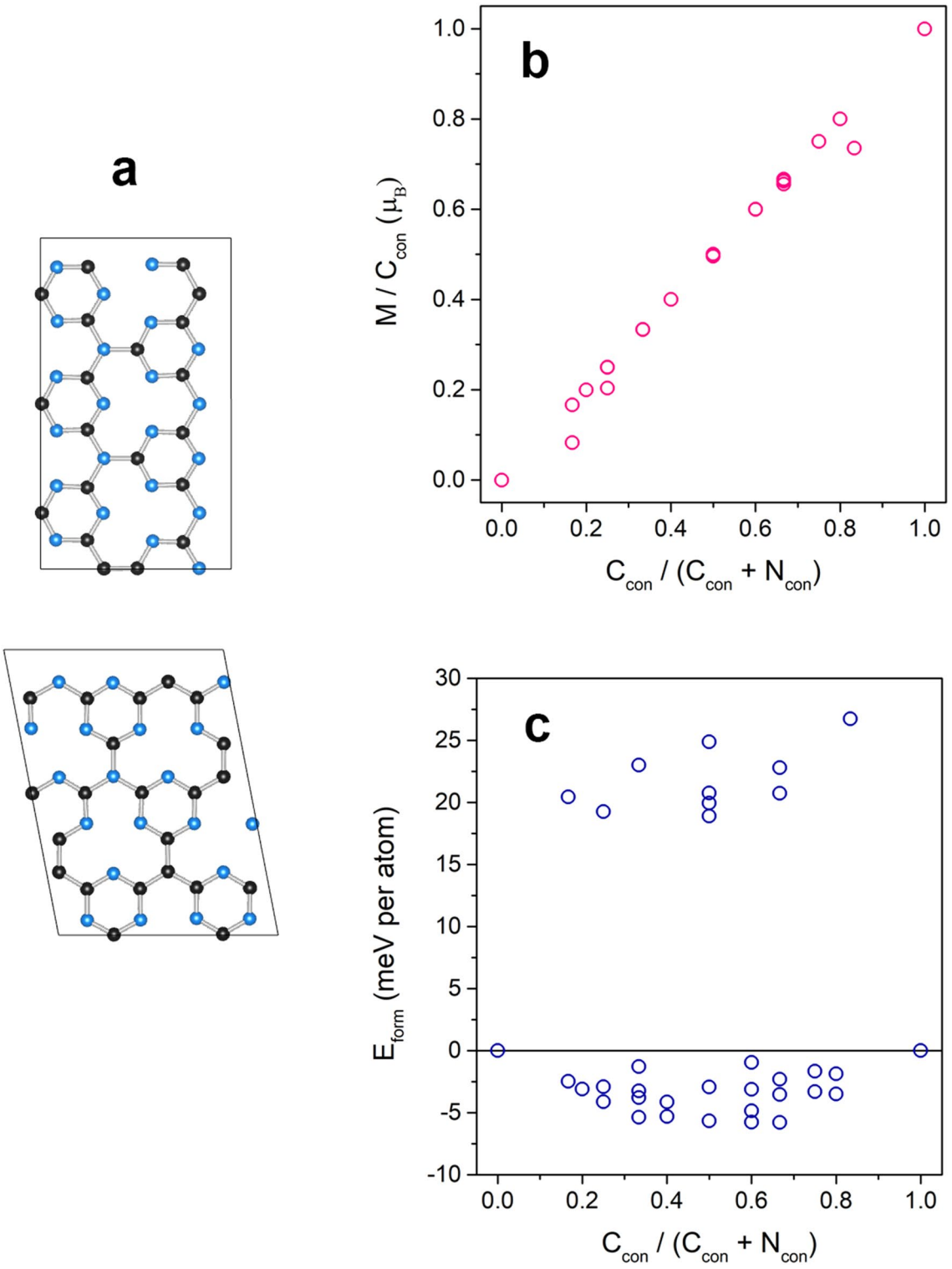

Figure 6. (**a**) Some order phases of TRI-C/N alloy are illustrated for a demonstration. (**b**) Magnetizations and (**c**) the formation energy of order phases compared with the energy of TRI-N and TRI-C are plotted with respect to the ratio between a number of C_{con} and a number of all connectors where C_{con} and N_{con} are C and N connectors. Noting that 0.0 and 1.0 in x-axis represent TRI-N and TRI-C, respectively.

		Cores					
		C	N	TRI	HEP	HEC	BEN
Connectors	C	–	0.00	0.00	0.00	1.00	0.20
	N		–	0.84	0.00	0.00	0.00
	TRI			1.00	0.00	0.00	0.00
	HEP				0.00	0.00	0.00
	HEC					1.00	1.00
	BEN						0.00

Table 4. The magnetization of each hydrogenated GCN is reported in μ_B unit where each column and row are core and connector components, respectively. The pink (grey) labels the phase that its magnetization does (not) different from its non-hydrogenated phase.

$$n(\mathbf{r}) = \sum_{\alpha} n^{\alpha\alpha(\mathbf{r})}, \quad \mathbf{m}(\mathbf{r}) = \sum_{\alpha\beta} \boldsymbol{\sigma}^{\alpha\beta} n^{\alpha\beta}(\mathbf{r}), \tag{1}$$

where $\boldsymbol{\sigma}$ is $(\sigma_x, \sigma_y, \sigma_z)$, a vector of the Pauli matrices and α and β are spin indices, spin up ($\uparrow$) or spin down ($\downarrow$). The collinear spin-polarization treats the spins to be aligned in the same direction, typically z direction, so $\boldsymbol{\sigma} = (0, 0, \sigma_z)$. The spin density matrix is thus

$$n^{\alpha\beta}(\mathbf{r}) = \frac{1}{2}(n(\mathbf{r})\delta^{\alpha\beta} + m_z(\mathbf{r})\sigma_z^{\alpha\beta}). \tag{2}$$

Therefore, the charge density and magnetization density, respectively, can be computed by

$$n(\mathbf{r}) = n^{\uparrow}(\mathbf{r}) + n^{\downarrow}(\mathbf{r}), \tag{3}$$

$$m(\mathbf{r}) = n^{\uparrow}(\mathbf{r}) - n^{\downarrow}(\mathbf{r}). \tag{4}$$

where $n^{\uparrow}$ and $n^{\downarrow}$ are eigenvalues of the spin density matrix solved by the Kohn–Sham equation[60].

The DFT calculation is used the projector augmented wave (PAW) method[61] for a pseudopotential and the Perdew–Berke–Erzenhof (PBE) for an exchange-correlation functional[62]. All calculations have been performed by including the van der Waals correction using Grimme DFT-D3 method[63]. The energy cutoff is 600 eV, and the k-point interval has been set to be 0.02 $Å^{-1}$ at most for every size of unit cell. The c-axis has been constrained to be 20 Å in order to avoid an interaction between layers. The tetrahedron method[64] has been performed to calculate the spin-polarized density of states (DOS).

The formation energy (E_{form}) of carbon nitrides and hydrogenated carbon nitrides systems per atom has been calculated using

$$E_{form}(C_xN_yH_z) = \frac{E(C_xN_yH_z) - 0.5[xE(C_2) + yE(N_2) + zE(H_2)]}{x + y + z}, \tag{5}$$

where $E(C_xN_yH_z)$ is the energy of $C_xN_yH_z$, and $E(C_2)$, $E(N_2)$, and $E(H_2)$ are the energy of graphene, N_2 molecule, and H_2 molecule, respectively.

Received: 18 June 2021; Accepted: 20 December 2021
Published online: 11 February 2022

References

1. Sethulakshmi, N. *et al.* Magnetism in two-dimensional materials beyond graphene. *Mater. Today* **27**, 107–122 (2019).
2. Choudhuri, I., Bhauriyal, P. & Pathak, B. Recent advances in graphene-like 2d materials for spintronics applications. *Chem. Mater.* **31**, 8260–8285 (2019).
3. Alcón, I. *et al.* Controlling pairing of π-conjugated electrons in 2D covalent organic radical frameworks via in-plane strain. *Nat. Commun.* **12**, 1705 (2021).
4. Bafekry, A., Neek-Amal, M. & Peeters, F. M. Two-dimensional graphitic carbon nitrides: Strain-tunable ferromagnetic ordering. *Phys. Rev. B* **101**, 165407. https://doi.org/10.1103/PhysRevB.101.165407 (2020).
5. Jiang, Y. *et al.* Organic radical-linked covalent triazine framework with paramagnetic behavior. *ACS Nano* **13**, 5251–5258 (2019).
6. Minkin, V. I. *et al.* Electronic structure and magnetic properties of the triangular nanographenes with radical substituents: A DFT study. *Phys. Chem. Chem. Phys.* **22**, 1288–1298 (2020).
7. Fernández-Rossier, J. & Palacios, J. J. Magnetism in graphene nanoislands. *Phys. Rev. Lett.* **99**, 177204. https://doi.org/10.1103/PhysRevLett.99.177204 (2007).
8. Arikawa, S., Shimizu, A., Shiomi, D., Sato, K. & Shintani, R. Synthesis and isolation of a kinetically stabilized crystalline triangulene. *J. Am. Chem. Soc.* PMID: 34767718.
9. Santiago, R. *et al.* 2d hexagonal covalent organic radical frameworks as tunable correlated electron systems. *Adv. Funct. Mater.* **31**, 2004584 (2021).
10. Lieb, E. H. Two theorems on the Hubbard model. *Phys. Rev. Lett.* **62**, 1201–1204. https://doi.org/10.1103/PhysRevLett.62.1201 (1989).
11. Yazyev, O. V. & Helm, L. Defect-induced magnetism in graphene. *Phys. Rev. B* **75**, 125408 (2007).

12. Rudenko, A. N., Keil, F. J., Katsnelson, M. I. & Lichtenstein, A. I. Exchange interactions and frustrated magnetism in single-side hydrogenated and fluorinated graphene. *Phys. Rev. B* **88**, 081405 (2013).
13. González-Herrero, H. *et al.* Atomic-scale control of graphene magnetism by using hydrogen atoms. *Science* **352**, 437–441 (2016).
14. Zhang, Y. *et al.* Scanning tunneling microscopy of the π magnetism of a single carbon vacancy in graphene. *Phys. Rev. Lett.* **117**, 166801 (2016).
15. Babar, R. & Kabir, M. Ferromagnetism in nitrogen-doped graphene. *Phys. Rev. B* **99**, 115442 (2019).
16. Fu, L. *et al.* Graphitic-nitrogen-enhanced ferromagnetic couplings in nitrogen-doped graphene. *Phys. Rev. B* **102**, 094406 (2020).
17. Shi, Z., Kutana, A. & Yakobson, B. I. How much n-doping can graphene sustain. *J. Phys. Chem. Lett.* **6**, 106–112 (2015).
18. Quan, L., Qin, F., Estevez, D., Wang, H. & Peng, H. Magnetic graphene for microwave absorbing application: Towards the lightest graphene-based absorber. *Carbon* **125**, 630–639 (2017).
19. Bu, S., Yao, N., Hunter, M. A., Searles, D. J. & Yuan, Q. Design of two-dimensional carbon-nitride structures by tuning the nitrogen concentration. *NPJ Comput. Mater.*https://doi.org/10.1038/s41524-020-00393-5 *(2020).*
20. Du, A., Sanvito, S. & Smith, S. C. First-principles prediction of metal-free magnetism and intrinsic half-metallicity in graphitic carbon nitride. *Phys. Rev. Lett.* **108**, 197207. https://doi.org/10.1103/PhysRevLett.108.197207 (2012).
21. Liu, L. Z., Wu, X. L., Liu, X. X. & Chu, P. K. Electronic structure and magnetism in g-C_4N_3 controlled by strain engineering. *Appl. Phys. Lett.* **106**, 132406. https://doi.org/10.1063/1.4916814 (2015).
22. Kamachi, M. Magnetic polymers. *J. Macromol. Sci. Part C* **42**, 541–561 (2002).
23. Kumar, S., Kumar, Y., Keshri, S. K. & Mukhopadhyay, P. Recent advances in organic radicals and their magnetism. *Magnetochemistry* **2**, 42 (2016).
24. Kroke, E. *et al.* Tri-s-triazine derivatives. Part I. From trichloro-tri-s-triazine to graphitic C_3N_4 structures. *New J. Chem.* **26**, 508–512. https://doi.org/10.1039/B111062B (2002).
25. Li, X., Zhou, J., Wang, Q., Kawazoe, Y. & Jena, P. Patterning graphitic C–N sheets into a kagome lattice for magnetic materials. *J. Phys. Chem. Lett.* **4**, 259–263. https://doi.org/10.1021/jz3018804 (2013) (**PMID: 26283431**).
26. Wang, A., Zhang, X. & Zhao, M. Topological insulator states in a honeycomb lattice of s-triazines. *Nanoscale* **6**, 11157–11162. https://doi.org/10.1039/C4NR02707H (2014).
27. Suter, T. *et al.* Synthesis, structure and electronic properties of graphitic carbon nitride films. *J. Phys. Chem. C* **122**, 25183–25194 (2018).
28. Chamorro-Posada, P. *et al.* Experimental and theoretical investigations on a CVD grown thin film of polymeric carbon nitride and its structure. *Diam. Relat. Mater.* **111**, 108169 (2021).
29. Inoki, H., Seo, G. & Kanai, K. Synthesis of graphitic carbon nitride under low ammonia partial pressure. *Appl. Surf. Sci.* **534**, 147569 (2020).
30. Zhu, J., Xiao, P., Li, H. & Carabineiro, S. A. C. Graphitic carbon nitride: Synthesis, properties, and applications in catalysis. *ACS Appl. Mater. Interfaces* **6**, 16449–16465. https://doi.org/10.1021/am502925j (2014) (**PMID: 25215903**).
31. LakshmanaReddy, N., Kumbhar, V. S., Lee, K. & Shankar, M. Chapter 9–Graphitic carbon nitride-based nanocomposite materials for photocatalytic hydrogen generation. In *Nanostructured, Functional, and Flexible Materials for Energy Conversion and Storage Systems* (eds Pandikumar, A. & Rameshkumar, P.) 293–324 (Elsevier, 2020).
32. Mpoutas, D. & Tsetseris, L. Magnetic two-dimensional C_3N_2 carbonitrides: Semiconductors, metals and half-metals. *Phys. Chem. Chem. Phys.* **19**, 26743–26748 (2017).
33. Choudhuri, I., Kumar, S., Mahata, A., Rawat, K. S. & Pathak, B. Transition-metal embedded carbon nitride monolayers: High-temperature ferromagnetism and half-metallicity. *Nanoscale* **8**, 14117–14126 (2016).
34. Xu, K. *et al.* Hydrogen dangling bonds induce ferromagnetism in two-dimensional metal-free graphitic-C_3N_4 nanosheets. *Chem. Sci.* **6**, 283–287 (2015).
35. Huanhuan, Q., Zhijun, W. & Xianlei, S. Ferromagnetism and antiferromagnetism in hydrogenated g-C_3N_4: A first-principles study. *Physica B Condens. Matter* **421**, 46–49 (2013).
36. Pawlak, R. *et al.* Bottom-up synthesis of nitrogen-doped porous graphene nanoribbons. *J. Am. Chem. Soc.* **142**, 12568–12573 (2020).
37. Gao, D. *et al.* Defect-related ferromagnetism in ultrathin metal-free g-C_3N_4 nanosheets. *Nanoscale* **6**, 2577–2581 (2014).
38. Bafekry, A., Shayesteh, S. F. & Peeters, F. M. Two-dimensional carbon nitride (2DCN) nanosheets: Tuning of novel electronic and magnetic properties by hydrogenation, atom substitution and defect engineering. *J. Appl. Phys.* **126**, 215104 (2019).
39. Bafekry, A., Shayesteh, S. F. & Peeters, F. M. Two-dimensional carbon nitride (2dcn) nanosheets: Tuning of novel electronic and magnetic properties by hydrogenation, atom substitution and defect engineering. *J. Appl. Phys.* **126**, 215104. https://doi.org/10.1063/1.5120525 (2019).
40. Gao, D. *et al.* Manifestation of high-temperature ferromagnetism in fluorinated graphitic carbon nitride nanosheets. *J. Mater. Chem. C* **3**, 12230–12235 (2015).
41. Verma, S., Nasir Baig, R. B., Han, C., Nadagouda, M. N. & Varma, R. S. Magnetic graphitic carbon nitride: Its application in the C–H activation of amines. *Chem. Commun.* **51**, 15554–15557 (2015).
42. Meng, B. *et al.* Half-metallic and magnetic properties in nonmagnetic element embedded graphitic carbon nitride sheets. *Phys. Chem. Chem. Phys.* **17**, 22136–22143 (2015).
43. Choudhuri, I., Garg, P. & Pathak, B. Tm@gt-C_3N_3 monolayers: high-temperature ferromagnetism and high anisotropy. *J. Mater. Chem. C* **4**, 8253–8262 (2016).
44. Liu, X. *et al.* Designing two-dimensional versatile room-temperature ferromagnets via assembling large-scale magnetic quantum dots. *Nano Lett.*. PMID: 34761940.
45. Geim, A. K. & Novoselov, K. S. The rise of graphene. *Nat. Mater.* **6**, 183–191 (2007).
46. Zhang, X., Zhao, M., Wang, A., Wang, X. & Du, A. Spin-polarization and ferromagnetism of graphitic carbon nitride materials. *J. Mater. Chem. C* **1**, 6265–6270 (2013).
47. Zhang, X. & Zhao, M. Prediction of quantum anomalous hall effect on graphene nanomesh. *RSC Adv.* **5**, 9875–9880 (2015).
48. Zhang, X., Wang, A. & Zhao, M. Spin-gapless semiconducting graphitic carbon nitrides: A theoretical design from first principles. *Carbon* **84**, 1–8 (2015).
49. Li, H. *et al.* Tensile strain induced half-metallicity in graphene-like carbon nitride. *Phys. Chem. Chem. Phys.* **17**, 6028–6035. https://doi.org/10.1039/C4CP05560H (2015).
50. Choudhuri, I., Bhattacharyya, G., Kumar, S. & Pathak, B. Metal-free half-metallicity in a high energy phase c-doped gh-C_3N_4 system: A high curie temperature planar system. *J. Mater. Chem. C* **4**, 11530–11539 (2016).
51. Döblinger, M. *et al.* Structure elucidation of polyheptazine imide by electron diffraction-a templated 2Dcarbon nitride network. *Chem. Commun.* 1541–1543 (2009).
52. Schlomberg, H. *et al.* Structural insights into poly(heptazine imides): A light-storing carbon nitride material for dark photocatalysis. *Chem. Mater.* **31**, 7478–7486 (2019).
53. Ovchinnikov, A. A. Multiplicity of the ground state of large alternant organic molecules with conjugated bonds. *Theoretica Chimica Acta* **47**, 297–304. https://doi.org/10.1007/BF00549259 (1978).
54. Mataga, N. Possible, "ferromagnetic states" of some hypothetical hydrocarbons. *Theoretica Chimica Acta* **10**, 372–376 (1968).
55. Hart, G. L. W. & Forcade, R. W. Generating derivative structures from multilattices: Algorithm and application to hcp alloys. *Phys. Rev. B* **80**, 014120. https://doi.org/10.1103/PhysRevB.80.014120 (2009).

56. Yang, Y. *et al.* In situ no-slot joint integration of half-metallic $C(CN)_3$ cocatalyst into g-C_3N_4 scaffold: An absolute metal-free in-plane heterosystem for efficient and selective photoconversion of CO_2 into CO. *Appl. Catal. B Environ.* **264**, 118470 (2020).
57. Kresse, G. & Furthmüller, J. Efficiency of Ab-Initio Total Energy Calculations for Metals and Semiconductors Using a Plane-Wave Basis Set. *Computat. Mater. Sci.* **6**, 15 (1996).
58. Kresse, G. & Furthmüller, J. Efficient iterative schemes for ab initio total-energy calculations using a plane-wave basis set. *Phys. Rev. B* **54**, 11169 (1996).
59. Zeller, R. Spin-polarized DFT calculations and magnetism. *Comput. Nanosci. Yours.* **31**, 419–445 (2006).
60. Kohn, W. & Sham, L. J. Self-Consistent Equations Including Exchange and Correlation Effects. *Phys. Rev.* **140**, A1133 (1965).
61. Blöchl, P. E. Projector augmented-wave method. *Phys. Rev. B* **50**, 17953 (1994).
62. Perdew, J. P., Burke, K. & Ernzerhof, M. Generalized Gradient Approximation Made Simple. *Phys. Rev. Lett.* **77**, 3865 (1996).
63. Grimme, S., Antony, J., Ehrlich, S. & Krieg, H. A consistent and accurate ab initio parametrization of density functional dispersion correction (DFT-D) for the 94 elements H-Pu. *J. Chem. Phys.* **132**, 154104 (2010).
64. Blöchl, P. E., Jepsen, O. & Andersen, O. K. Improved tetrahedron method for Brillouin-zone integrations. *Phys. Rev. B* **49**, 16223 (1994).

Acknowledgements

This research project was supported by the Second Century Fund (C2F), Chulalongkorn University. This Project is partially funded by National Research Council of Thailand (NRCT): (NRCT5-RSA63001-04) and Ratchadaphiseksomphot Endowment Fund of Chulalongkorn University, Grant for Research. The financial support is also provided by Thailand Science Research and Innovation (TSRI) and Synchrotron Light Research Institute (SLRI). The Computational Materials Physics (CMP) Project, SLRI, Thailand, is acknowledged for providing computational resource.

Author contributions

Author contributions: T.P., and T.B. designed the research; T.P., A.E., A.S. and T.B. performed the research; T.P., A.E., U.P., and T.B. analysed the data; and T.P., U.P., and T.B. wrote the paper.

Competing interests

The authors declare no competing interests.

Additional information

Supplementary Information The online version contains supplementary material available at https://doi.org/10.1038/s41598-022-05590-4.

Correspondence and requests for materials should be addressed to T.B.

Reprints and permissions information is available at www.nature.com/reprints.

Publisher's note Springer Nature remains neutral with regard to jurisdictional claims in published maps and institutional affiliations.